Available online at www.sciencedirect.com

ScienceDirect

journal homepage: www.elsevier.com/locate/he

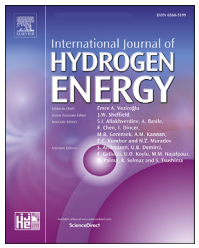

Mitigating high temperature hydrogen attack with interphase precipitation

M.A.M. Alshahrani [a,b,*], S.W. Ooi [c,d], G. Divitini [a,e], H.K.D.H. Bhadeshia [a,f]

[a] University of Cambridge, Materials Science and Metallurgy, Cambridge, CB2 3QZ, United Kingdom
[b] Saudi Aramco, Research and Development Centre, Dhahran 34466, Saudi Arabia
[c] Ovako Corporate R&D, Maxwell Centre, University of Cambridge, JJ Thomson Avenue, Cambridge, CB3 0HE, United Kingdom
[d] Ovako Sweden, Building 303, 81382 Hofors, Sweden
[e] Istituto Italiano di Tecnologia, Electron Spectroscopy and Nanoscopy, Genova 16163, Italy
[f] Queen Mary University of London, School of Engineering and Materials Science, London, E1 4NS, United Kingdom

HIGHLIGHTS

- Isothermally heat-treated vanadium steel was shown to mitigate hydrogen attack.
- Vanadium carbides reduced carbon activity, hence resisted depletion by hydrogen.
- Undesirable martensite formation led to high carbon activity and methane formation.
- Heat treatment is a must-include parameter in standards to reduce carbon activity.

ARTICLE INFO

Article history:
Received 24 June 2023
Received in revised form
15 September 2023
Accepted 17 September 2023
Available online 04 October 2023

ABSTRACT

The attack on steel by reaction with high-pressure hydrogen at elevated temperatures can jeopardise structural integrity in oil & gas industries. Following dissociation, the hydrogen penetrates the steel to react with the carbon present in the ferrite to form methane bubbles within the microstructure. This depletion of carbon in the ferrite causes the dissolution of carbides in order to maintain the ferrite-carbide equilibrium. Therefore, thermodynamically more stable carbides which cause a reduced activity of carbon improve the stability of the steel to hydrogen attack. In this work, we investigate specifically the response of the interphase precipitation of alloy carbides that form during the transformation from γ to α, on hydrogen attack. It is demonstrated quantitatively that the vanadium carbides thus produced enhance the resistance to attack when compared with data from an earlier study involving current, commercially-used steel in the petrochemical industries.

* *Corresponding author*. Saudi Aramco, Research and Development Centre, Dhahran 34466, Saudi Arabia.
E-mail addresses: mohammed.shahrani.34@aramco.com, m.shahrani91@hotmail.com (M.A.M. Alshahrani).

https://doi.org/10.1016/j.ijhydene.2023.09.179

1. Introduction

Some steel components in the petrochemical industries come into contact with gaseous hydrogen at high pressures and temperatures. The dissociation and entry of nascent hydrogen into the steel can then lead to a form of "attack" that involves its reaction with carbon to form methane bubbles within the microstructure. The consequent damage can be debilitating or catastrophic, as at the Tesoro Anacortes Refinery [1–14].

The methane reaction can be written as follows:

$$[C]_\alpha + 4[H]_\alpha \rightarrow [CH_4]_{gas} \quad (1)$$

where α refers to ferrite. The concentration of carbon within the ferrite is, prior to attack, related to its equilibrium with any carbides with which it is in contact. So if that carbon becomes depleted by reaction with the hydrogen in the ferrite, then the carbides dissolve to replenish the equilibrium. Hydrogen can move rapidly in ferrite so the attack would then be focused in the vicinity of the carbide, with methane creating cavities where the carbides previously existed. The *effective* reaction is therefore often written as

$$Fe_3C + 4[H]_\alpha \rightarrow [CH_4]_{gas} + 3Fe \quad (2)$$

For the case where cementite is the principal carbide. More thermodynamically stable carbides lead to a smaller carbon activity in the steel and hence greater resistance to attack [15,16].

The purpose of the present work is to use the concept of *interphase precipitation* [17,18] to create an array of stable alloy-carbides, during the growth of ferrite from austenite. Because the transformation occurs at a temperature greater than normally used for tempering, the carbides that do precipitate are more stable. The precipitation actually occurs during the piecewise advance of the γ/α interface by a step mechanism. The alloy system selected here leads to the fine precipitation of vanadium carbides, which are known to help resist creep deformation [19]. The hydrogen-attack resistance is also compared against our previous work on the classical 2.25Cr–1Mo steel [16].

2. Experimental procedure

The design of the experiments in this work is based on choosing a steel with a stoichiometric composition, that is isothermally heat-treated to produce only interphase-precipitation carbides. The steel is then exposed to an environment that induces the attack. The characterisation of the carbides is done before and after the exposure to assess the resistance of the steel. A more detailed explanation of the experimental matrix follows in this section.

2.1. Material and heat treatment

According to the famous "Nelson Curves", the addition of vanadium enhances the hydrogen attack resistance of 2.25Cr–1Mo steel. Vanadium is also known to introduce interphase precipitation, if the appropriate heat treatment is followed [20,21]. Therefore, the only alloying element added to the steel in this work is vanadium.

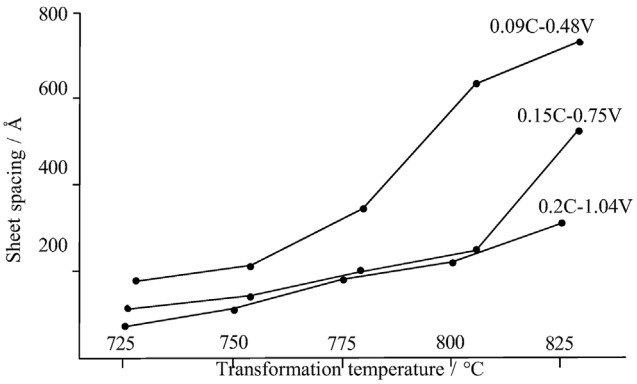

Fig. 1 – Effect of transformation temperature on the sheet spacing of vanadium carbides in different vanadium steels. Adapted from Ref. [21] with permission of Taylor & Francis.

The main idea driving the experimental procedure is minimizing the free carbon, i.e. carbon activity. Therefore, the composition was chosen based on the work of Honeycombe and Batte [21] with the intention of precipitating the highest vanadium carbide volume fraction, which was detected in a 0.2C-1.04V steel (wt%). Thus, 0.2C-1.04V steel was manufactured and examined in this work. This composition is also stoichiometric, which ensures that all the carbon is tied up in the stable carbides upon the completion of transformation, leading to the minimal carbon activity in the microstructure and prohibiting the concentration of carbon in untransformed austenite that would transform to martensite upon quenching [19].

The carbide dispersion is an important parameter in interphase precipitation that varies depending on the isothermal transformation temperature. To reiterate, the carbide sheets form with the movement of the γ/α interface by a step mechanism, which determines the sheet spacing. If the transformation temperature is decreased, the step height should decrease due to greater driving forces at larger undercoolings, hence the precipitation of finer spacing, as seen in Fig. 1 [18,22–26].

The heat treatments were carried out with the use of the dilatometer where steel specimens were austenitised at

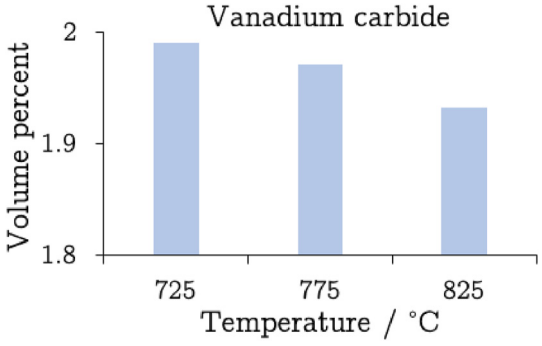

Fig. 2 – Equilibrium calculations of the volume fraction of vanadium carbide at different transformation temperatures. The residual phase is α.

Table 1 – *ThermoCalc* prediction of equilibrium chemical compositions (wt%) for vanadium carbides at different transformation temperatures in vanadium steel.

Element	725°C	775°C	825°C
C	16.68	16.72	16.75
Fe	6.38	6.48	6.47
V	76.93	76.79	76.78

1200°C for 15 min to ensure that all vanadium carbides are dissolved. The temperature then was dropped to the desired transformation temperature and kept there for 5 min to allow carbide precipitation, before quenching to room temperature. The transformation temperatures were 725°C, 775°C and 825°C.

2.2. *Hydrogen exposure*

The facility at The Welding Institute (TWI) was used to expose the steel specimens to hydrogen for 500 h at 525°C and 10 MPa of hydrogen pressure. The specimens were placed within three large cylinders of 316L stainless steel, which then was placed at the centre of a tube furnace. A total of six specimens were exposed to hydrogen; two specimens at each transformation temperature mentioned above. The specimens heat-treated at the same temperature were placed next to each other. These conditions are exactly the same as the ones followed in the previous investigation on 2.25Cr–1Mo [16] in order to compare the results of interphase-precipitation steels to commercially used steels.

2.3. *Characterisation*

The steel was characterised before and after hydrogen exposure. Three parameters were characterized and correlated in this work to assess the resistance of the steel to hydrogen attack:

- the volume fraction of voids due to methane formation after hydrogen exposure, which can be measured using *ImageJ* on micrographs taken by optical microscopy. It is important to keep in mind that inclusions might be present in the steel and mistaken for voids when processing the micrographs, therefore, volume fraction of inclusions was measured before hydrogen exposure and subtracted from the volume fraction of voids that were measured after the exposure. The void volume fraction measured here provides initial evidence of whether or not the steel had undergone hydrogen attack.
- The reactants for methane formation in hydrogen attack are hydrogen and the carbon in carbides, therefore, if the volume fraction of carbides decreases upon hydrogen exposure, the steel is considered to have undergone hydrogen attack. Carbide volume-fractions were measured

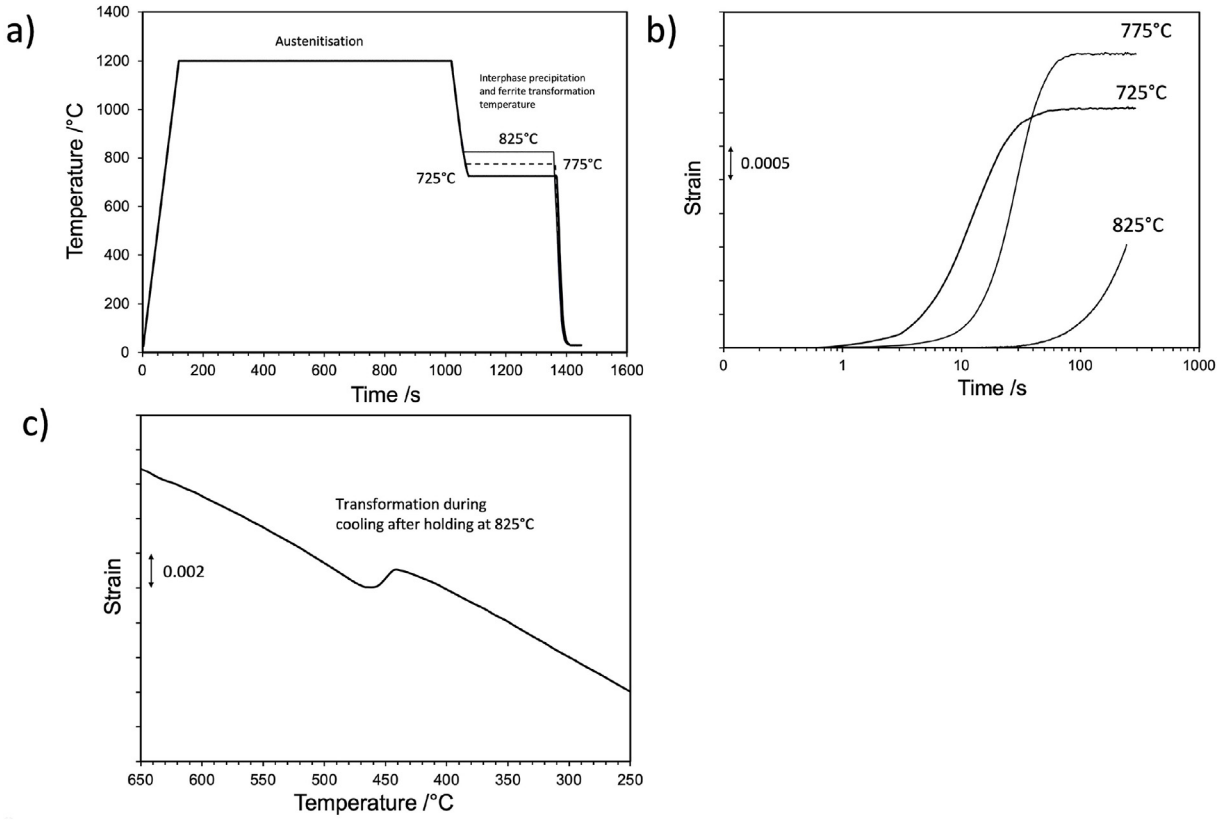

Fig. 3 – a) A representation of all heat treatments including heating to austenitisation temperature followed by cooling to the isothermal transformation temperature then cooling to room temperature. b) The strain detected throughout the heat treatment for all specimens. c) The strain detected during cooling to room temperature in the specimen isothermally transformed at 825°C, where the strain increase is due to martensite formation.

using synchrotron X-ray analysis before and after the exposure. Synchrotron X-ray provides evidence of the extent of depletion. Experiments were conducted on The Diamond Light Source Beamline I12 in the United Kingdom. The X-ray wavelength was 0.2066 Å, monochromated using diffraction. The sample detector distance was determined to be 2800 mm to allow the largest possible diffraction at $2\theta < 15^{\circ}$, where the most intense peaks of carbides are expected. The X-ray beam size was chosen to be 0.5 mm×0.5 mm with a dwell time of 7 s per measurement point. Hundreds of images were captured, spaced out evenly across each specimen. Analysis was performed using Python modules; pyFAI-calib2 and pyFAI-integrate for detector calibration and data reduction respectively. Rietveld analysis using *MAUD* [27] was used to calculate the volume-fraction of carbides.

- Confirmation of interphase precipitation was done using transmission electron microscopy; FEI Tecnai Osiris FEG TEM, fitted with an energy dispersive spectroscopy to measure the chemical composition of the carbides. It is important to measure the latter to check how close the composition is to equilibrium compositions as calculated by ThermoCalc, as it was shown in previous work [16] that equilibrium conditions influence the resistance to hydrogen attack. Scanning electron microscopy and optical microscopy were also used for microstructural analysis.

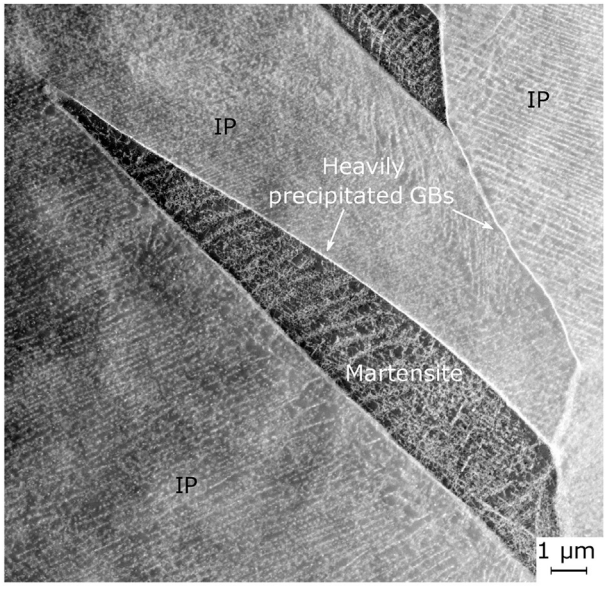

(a)

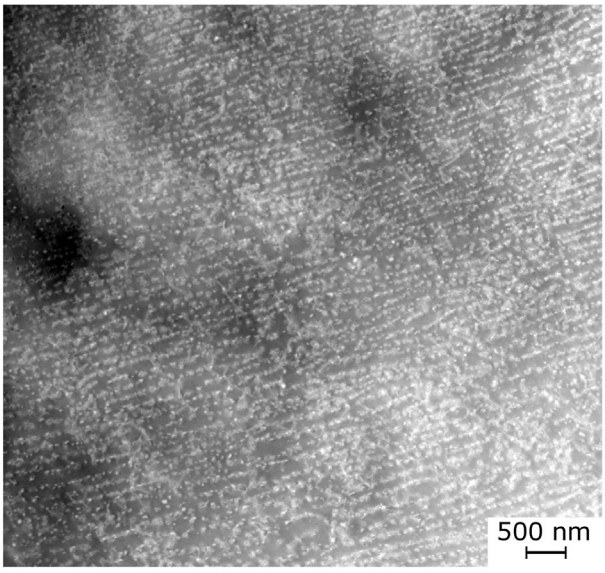

(b)

Fig. 4 – a) TEM dark field image for vanadium steel transformed isothermally at 825°C for 5 min showing ferritic regions with interphase precipitates (IP) in rows as well as martensite. b) A magnified dark field image of interphase precipitation in the same specimen.

2.4. *Equilibrium calculations*

ThermoCalc (TCFE10 database) was used to estimate equilibrium carbide volume-fractions as well as their equilibrium compositions at different transformation temperatures. These estimations represent thermodynamic equilibrium rather than kinetics but can nevertheless give useful information.

Vanadium carbides are the only carbides expected to precipitate in this steel. In the calculations using *ThermoCalc*, in a Fe–C–V system, MC was allowed to exist alongside ferrite and austenite. As the transformation temperature increases, the MC volume fraction is seen to slightly decrease, Fig. 2. However, the differences for the temperatures considered are not large given the exaggerated scale on the vertical axis. In a system constrained to two phases existing simultaneously, in this case $\alpha + MC$, variations in phase fractions are determined entirely by changes in the chemical composition of the phases as a function of temperature. Since the equilibrium concentration of carbon in ferrite is quite small at all temperatures, the fraction of carbide cannot change much with temperature.

The composition of vanadium carbide at the transformation temperatures is listed in Table 1. The change in composition is also slight at the different transformation temperatures. The small change in volume fractions and compositions between the transformation temperatures could suggest that the transformation temperature will mainly influence the interphase-precipitation carbide size and sheet spacing.

3. Results and discussion

3.1. *Characterisation after the heat treatment*

3.1.1. *Microstructure*

Because of the isothermal transformation followed in this work, a ferritic microstructure is expected in all of the specimens. The change in strain detected by the dilatometer could

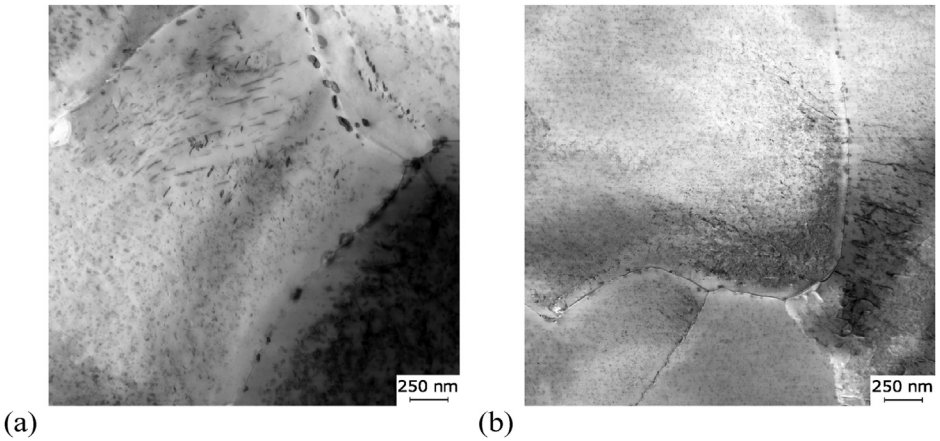

Fig. 5 – TEM bright field images for vanadium steel transformed isothermally at a) 775°C for 5 min, b) 725°C for 5 min. Precipitates at grain boundaries are larger at higher transformation temperatures. Precipitate-free zones can be seen around grain boundaries.

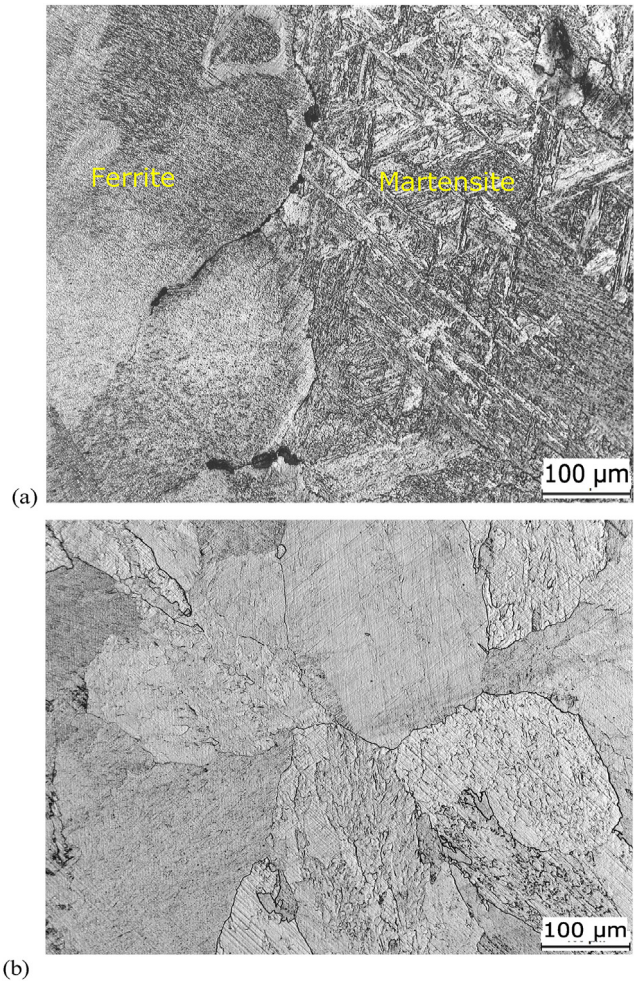

Fig. 6 – Micrographs of vanadium steel microstructure transformed isothermally at a) 825°C, showing two different phases, martensite and ferrite. b) 725°C, showing one phase, i.e. ferrite.

be an indication of the microstructure expected, which is shown for all specimens in Fig. 3a. Transformation from one phase to another is accompanied by a change in the macroscopic volume of the specimen, therefore, when no change in strain is detected any longer, then the transformation is assumed to be completed. As can be seen from Fig. 3b, the strain detected for the specimens isothermally-transformed at 725°C and 775°C reaches a plateau, suggesting that the transformation is completed, which is not the case for the specimen isothermally-transformed at 825°C, which means that the transformation to ferrite in the latter specimen is not completed. Fig. 3c shows the change in strain detected for the specimen isothermally transformed at 825°C during cooling to room temperature. This change is an indication of the martensite formation.

The microstructures were then analysed using transmission electron microscopy. Fig. 4a shows very fine interphase precipitation in the ferritic region of the specimen that was isothermally transformed at 825 °C, as well as the martensitic microstructure. It can also be seen in Fig. 4a that prior austenite grain boundaries contain heavy precipitation in this condition. Grain boundaries are regions of high internal energy, which make them preferred sites for precipitation, which explains why grain boundaries are associated with exaggerated precipitation. The same behaviour is observed at lower transformation temperatures, Fig. 5, though to a lesser extent presumably because of the slower precipitation kinetics. The scale of the

Table 2 – Micro-hardness measurements of isothermally transformed vanadium steel at different temperatures.

Specimen	Hardness ($HV_{0.1}$)	Phase
A (725 °C)	354 ± 3	Ferrite
B (775 °C)	271 ± 3	Ferrite
C (825 °C)	161 ± 3	Ferrite
	325 ± 4	Martensite

Table 3 – Void/inclusion volume-fractions before and after hydrogen exposure for vanadium steel. The quantities for the exposed specimens include the voids fraction from the unexposed state. IT refers to isothermal transformation, which was for 5 min for vanadium steel. The error bars were calculated by dividing the standard deviation by the square root of the number of measurements.

Specimen	V_V
Unexposed	$11 \times 10^{-6} \pm 2 \times 10^{-6}$
ITa (725°C)	$19 \times 10^{-6} \pm 3 \times 10^{-6}$
ITb (775°C)	$16 \times 10^{-6} \pm 5 \times 10^{-6}$
ITc (825°C)	$32 \times 10^{-6} \pm 8 \times 10^{-6}$

Underlined volume fraction is used to diffrentiate between unexposed and exposed specimens.

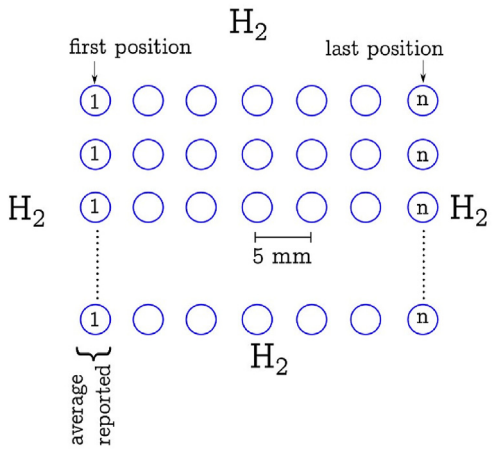

Fig. 7 – A representation of how measurements are taken with synchrotron X-ray for hydrogen-exposed specimens. The positions shown correspond to those listed in Table 4 with n being the last position.

microstructure decreases with decreasing transformation temperature as the accompanying diffusion distances are reduced. Grain boundary precipitation depletes the solute in the adjacent vicinity introducing precipitate-free zones around them, as can be seen clearly in Fig. 5a in the vicinity of the grain boundaries.

Using optical microscopy, two clearly distinguished phases were seen in the specimen transformed isothermally at 825°C; martensite and ferrite as can be seen in Fig. 6a, while only ferrite can be identified in Fig. 6b, corresponding to the steel transformed isothermally at 725°C.

The incomplete transformation from austenite to ferrite is undesirable in this application because it means that not all available carbon has been tied up in carbides, therefore, carbon activity is not at minimum, hence methane formation is more likely to occur. The effect of the incomplete transformation will be discussed later.

A substructure can be in seen in ferritic phase in Fig. 6b. There is significant work to show crystallographic orientation gradients, using electron back-scattered diffraction on Fe–C–V–Mn–Si and other steels that are transformed to generate ferrite containing interphase precipitation.

Such orientation gradients arise because the ferrite nucleates at grain junctions and can grow into all of the adjacent austenite grains, albeit the different rates. The ferrite possesses a coherent orientation with only one such grain and grows more rapidly into austenite grains with which it has relatively incoherent boundaries. This is responsible for the substructure visible in optical micrographs and a similar example is in the work of Wang et al. [28]. It is likely therefore, that the contrast seen in our figure arises for the same reason, though we have not done the work to show that since that was not the main objective.

3.1.2. *Hardness*

Martensite formation can be further supported by analysing the hardness of the different phases. Micro-hardness testing was carried out on all specimens and the results are shown in Table 2. The highest hardness of ferrite is measured at the lowest transformation temperature, as expected, due to the finer dispersion of carbides as witnessed in different studies [19,23,26]. The micro-hardness measurements were uniform across the specimens transformed at 725°C and 775°C, on the other hand, a large difference was detected between the two distinguished phases in the specimen transformed at 825°C. The relative fractions of the phases can be estimated using the following equation [29]:

$$V_V^{\alpha} \approx \frac{HV_{\alpha^l} - HV}{HV_{\alpha^l} - HV_{\alpha}} \tag{3}$$

where HV_{α}^{l} is the hardness of freshly quenched martensite, HV_{α} is the hardness of a fully ferritic specimen. HV_{α}^{l} was calculated by quenching a specimen to be 386 $HV_{0.1}$, HV_{α} was taken to be the ferrite hardness in specimen C, while HV is the average hardness in specimen C, equaling 243 $HV_{0.1}$. This estimates the ferrite volume fraction of 0.63, leaving 0.37 as martensite in specimen C.

As can be seen from Table 2, the microhardness in the ferritic specimen A is higher than that of the martensite phase in specimen C, which can be the consequence of the dense precipitation of vanadium carbides in specimen A. A study by Miyatomo et al. measured the hardness of vanadium steel with varying vanadium compositions when the steel was isothermally transformed at different temperatures for different durations. They found that hardness increases as the transformation temperature decreases especially when the vanadium content is higher than 0.1 wt% [20], which agrees with the findings in this work. The steel composition along with the conditions of isothermal transformation in Miyamoto's work are different from the conditions in this work, therefore the hardness values could not be compared directly. However, for a 0.44C-0.1V (wt%) steel, which is less than the vanadium used in this work, a minimum of 250 HV and a maximum of 280 HV was achieved. The hardness increases significantly when the vanadium content was increased to 0.3 wt% to reach a maximum of around 400 HV [20].

Table 4 – Synchrotron-measured carbide volume-fractions of MC carbide in vanadium steel specimens before and after hydrogen-exposure.

	725°C	775°C	825°C
Unexposed	0.0098 ± 0.0012	0.0095 ± 0.0003	0.0062 ± 0.0007
AE (1)	0.0086 ± 0.0015	0.0108 ± 0.0017	0.0036 ± 0.0009
AE (2)	0.0082 ± 0.001	0.0109 ± 0.0018	0.0036 ± 0.0012
AE (3)	0.0084 ± 0.0014	0.0101 ± 0.0015	0.004 ± 0.0014
AE (4)	0.0096 ± 0.0018	0.0108 ± 0.0009	0.0036 ± 0.0015
AE (5)	0.0106 ± 0.0017	0.0099 ± 0.0014	0.0059 ± 0.0018
AE (6)	0.0107 ± 0.0025	0.0104 ± 0.0018	0.0063 ± 0.0018
AE (7)	0.0093 ± 0.0017	0.0094 ± 0.0017	0.0079 ± 0.0019
AE (8)	0.0106 ± 0.0015	0.0092 ± 0.0013	0.0077 ± 0.002
AE (9)	0.0091 ± 0.0019	0.0104 ± 0.0012	0.0055 ± 0.002

Underlined are the positions where carbide depletion has occurred.

3.2. *Characterisation after hydrogen exposure*

3.2.1. *Void volume-fractions*

Now that interphase precipitation has occurred in the tested specimens, investigations on their hydrogen attack resistance can be carried out. According to previous work [16], and under the same hydrogen exposure conditions, void volume-fractions (V_V) in 2.25Cr–1Mo specimens have increased after exposure by a minimum of 25 × 10^{-5} and a maximum of 112 × 10^{-5} depending on the heat treatment. It should be highlighted that 2.25Cr–1Mo is the commercially-used steel when designing against hydrogen attack. V_V was measured for interphase-precipitated vanadium steel using the same methodology followed for 2.25Cr–1Mo steel. As can be seen from Table 3, the void volume-fraction has increased across vanadium steel specimens by 5 × 10^{-5} to 21 × 10^{-5}. These results clearly show the superior hydrogen attack resistance in interphase-precipitation vanadium steel to the commercially-used steel for hydrogen attack application, 2.25Cr–1Mo.

The above results show that specimens transformed isothermally at 725°C and 775°C exhibited better resistance than the specimen transformed at 825°C, which is not surprising considering the higher carbon activity expected in the undesirable formation of martensite in the latter specimen. Nonetheless, this isothermally-transformed specimen has shown a lower increase in void volume-fraction than the best performing specimen in 2.25Cr–1Mo in previous work [16], which could indicate the better resistance of vanadium carbides to carbides present in 2.25Cr–1Mo. Synchrotron X-rays analysis was done to examine the volume fraction of carbides before and after hydrogen-exposure in the following section.

3.2.2. *Volume fraction of carbides*

Synchrotron X-rays were used to compare the carbide volume fractions before and after hydrogen-exposure. The specimens were analysed horizontally from surface to surface with a distance of 0.5 mm between every measurement point in the same row, following the representation in Fig. 7. All values in

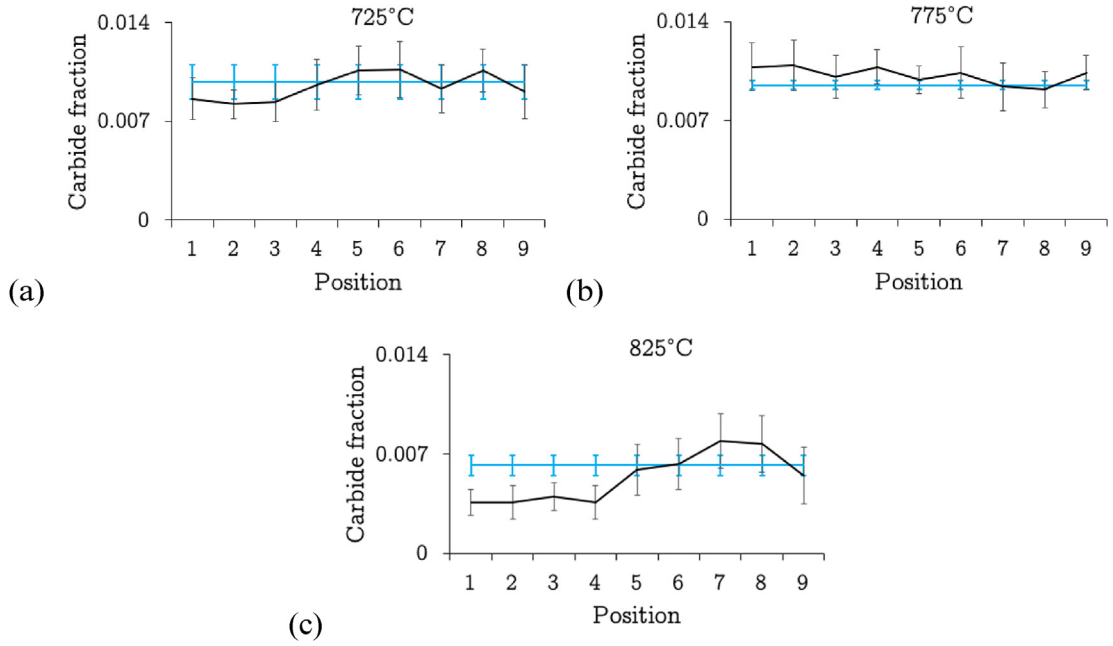

Fig. 8 – a, b and c) Volume fraction of MC carbide in vanadium steel transformed isothermally at different temperatures for 5 min. The average carbide fractions prior to exposure are represented with the standard deviation calculation by the blue lines, which were measured across the full specimen before hydrogen exposure. (For interpretation of the references to colour in this figure legend, the reader is referred to the Web version of this article.)

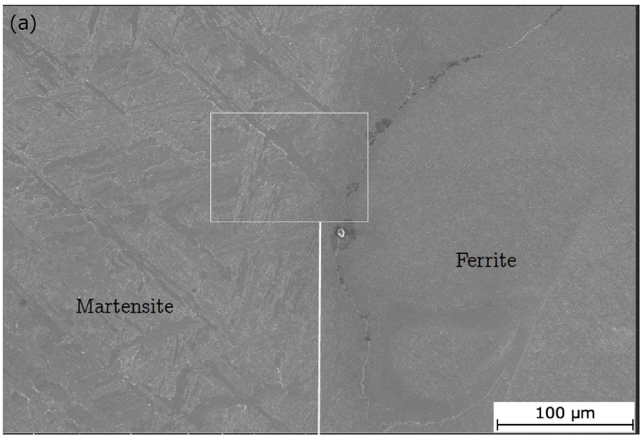

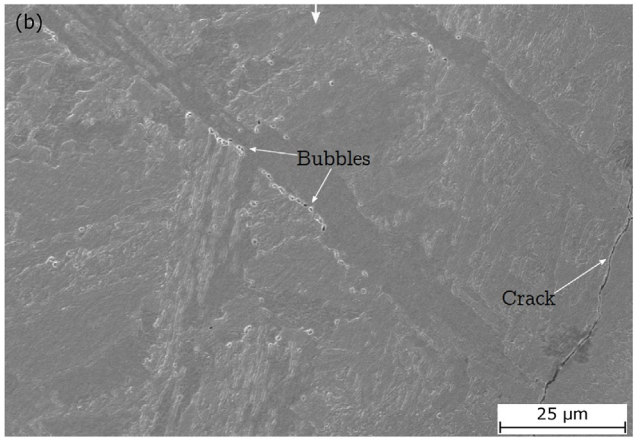

Fig. 9 – SEM micrographs of polished vanadium steel specimens showing the microstructure transformed isothermally at 825°C, showing two different phases, martensite and ferrite. Cracks are observed at the interface, while bubbles are seen across the martensitic phase. a) A micrograph showing both phases with cracks developing at the interface. b) A magnified micrograph.

the same position are averaged to one value for that position, which is then analysed by Rietveld analysis to calculate the fraction of carbides at that position.

Table 4 lists the analysis of the MC carbide volume fractions in all specimens before and after hydrogen exposure, while Fig. 8 is a representation of those fractions. MC carbide did not undergo any depletion after being exposed to high hydrogen pressures when the transformation was completed, at 725°C and 775°C, which agrees with the void volume-fraction measurements in Table 3. However, a noticeable reduction in MC carbide fraction was detected in the specimen transformed isothermally at 825°C,

Fig. 8c. The depletion seen in is expected to have occurred in the martensitic region of the specimen or at the ferrite/martensite interface, which can be seen in Figs. 9 and 10.

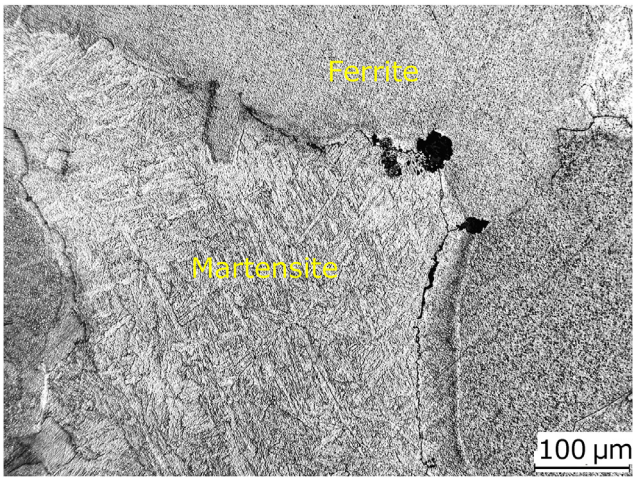

Fig. 10 – A micrograph of vanadium steel microstructure transformed isothermally at 825°C, showing two different phases, with cracks developing around and in the martensitic phase.

3.2.3. *Chemical composition of carbides*

Energy dispersive X-ray analysis in transmission electron microscopy was used to measure the chemical composition of vanadium carbides, then compared with the equilibrium compositions and volume fractions estimated by *ThermoCalc*. As can been from Tables 5 and 6, neither the volume fraction of MC carbide nor its composition is close to equilibrium, yet no depletion can be detected for MC carbide upon exposure to hydrogen, where isothermal transformation to ferrite was completed. The vanadium composition of the carbides is expected here to be qualitative as the precipitates are smaller than the probed depth. The vanadium content in the MC carbide in specimen C is much less than that found in the other two specimens, which suggests that it is further from equilibrium. Nonetheless, the depletion seen here is less than seen in the recent investigation in 2.25Cr–1Mo [16], where carbides have depleted more noticeably than specimen C when they were not at equilibrium. This indicates the superior resistance of vanadium carbides to that of chromium carbides when it comes to their resistance to be dissociated by hydrogen, which could correlate with the fact that vanadium enhances tensile strength and creep-rupture strength at high temperatures [30], thus limiting the power-law creep mechanism of hydrogen attack.

As mentioned before, precipitation is expected to be finer in spacing and size as the transformation temperature decreases, but that does not seem to influence the hydrogen attack resistance. The peaks in the synchrotron X-ray diffraction patterns were analysed (see Fig. 11) and it was observed that peaks were broader as the transformation temperature was reduced. This is due to the larger coherency strain field associated with the smaller particle size [31,32]. Therefore, it can be safe to say that the particles in the specimen transformed isothermally at 725°C were finer than the

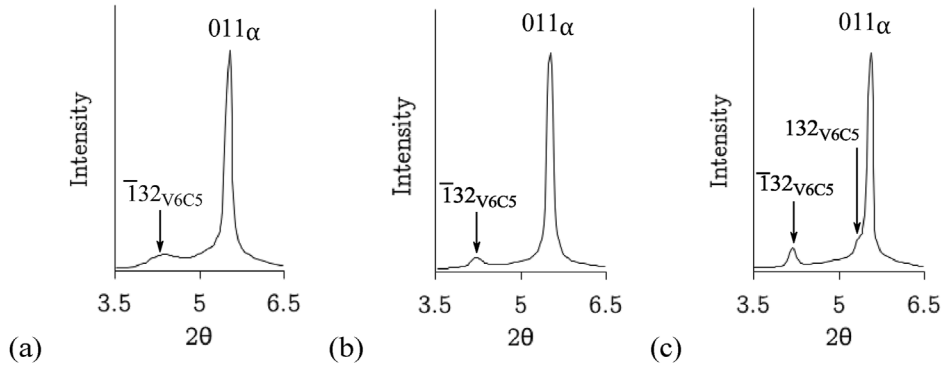

Fig. 11 – Synchrotron X-ray diffractograms of vanadium steel specimens transformed isothermally at a) 725°C, b) 775°C and c) 825°C. The broad peaks for the V_6C_5 carbides indicate finer precipitation.

Table 5 – Volume fractions of MC carbide as expected under equilibrium using *ThermoCalc* (T.C.) and as determined using synchrotron X-ray diffraction for isothermally transformed vanadium steel.

Temperature	MC	
	T.C.	Rietveld
725 °C	0.0199	0.0098 ± 0.0012
775 °C	0.0197	0.0095 ± 0.0003
825 °C	0.0193	0.0062 ± 0.0007

Table 6 – Equilibrium and measured chemical compositions (wt%) of MC carbide in vanadium steel at different isothermal transformation (IT) temperatures. *ThermoCalc* is used to calculate the equilibrium composition. EDX in TEM was used to measure the actual chemical composition. As carbon content cannot be accurately measured using EDX, all the carbon content values are calculated by *ThermoCalc* and EDX measurements for other elements were corrected accordingly.

	Specimen B IT @ 775 °C for 5 min		Specimen C IT @ 825 °C for 5 min	
	T.C.	EDX	T.C.	EDX
C	16.72	–	16.75	–
Fe	6.48	64.44 ± 2.01	6.47	78.81 ± 0.18
V	76.79	18.83 ± 0.92	76.78	4.34 ± 0.04

ones precipitated at 825°C, nonetheless, that did not prove to influence the hydrogen attack resistance.

4. Conclusions

Minimizing carbon activity in the steel is a critical step towards mitigating high temperature hydrogen attack. This work has shown, for the first time, that isothermal transformation of the steel is a better alternative to conventional heat treatments when it comes to hydrogen attack resistance. The principal conclusions are as follows:

- Vanadium has been used previously as an addition to commercially-used steels to increase the resistance to hydrogen attack. Vanadium in this work was used as the only alloying-element, and it exhibited excellent resistance to hydrogen attack. The resistance was also excellent when the carbides were far from their equilibrium state, unlike the commercially-used steel, 2.25Cr–1Mo steel, where equilibrium conditions had to be ensured to avoid any noticeable depletion in carbides [16]. This is a significant result as it challenges the current paradigm that classifies chromium as a necessary element in the steel to resist hydrogen attack.
- A major outcome from this work was the confirmation of the importance of heat treatment towards mitigating hydrogen attack. Interphase precipitation has produced steels that resist hydrogen attack better than steels that are heat-treated via conventional methods, keeping in mind that both steels were exposed to the same temperature and hydrogen pressure for the same duration. Only undesirable conditions in the interphase precipitation deteriorated the resistance of vanadium steel, when the austenite to ferrite transformation was incomplete, leading to the formation of untempered martensite with high carbon activity, which is the main catalyst for the formation of methane bubbles. It should be mentioned that interphase precipitation also required shorter tempering durations, i.e. less energy.
- Interphase precipitation of vanadium steel mitigated hydrogen attack mainly due to the minimisation of carbon activity by tying up all carbon with stable carbides directly at the γ/α moving interface. It is speculated that direct precipitation at the γ/α interface leaves the ferrite immediately depleted of carbon. On the other hand, conventional quench/temper heat-treated microstructures contain lattice defects, which may retain excess carbon that is available to react with hydrogen for methane formation. Vanadium is also known for its improvement on tensile strength and creep-rupture at high temperatures, which may be a factor in limiting the linkage of voids formed due to the methane formation.

Further research is needed to establish that the suggested vanadium steel as a viable alternative in hydrogen-attack

applications as a whole basket of other properties need to be satisfied:

- the mechanical properties of vanadium steel need to be characterised and compared with steel requirements to be deployed as components operating in high-temperature high-pressure hydrogen environments. This is a major step requiring industrial involvement in the definition of the work as this alloy was chosen because it was shown that it undergoes interphase precipitation, but it is not necessarily optimum for creep and oxidation-resistant applications, therefore experimental work is needed to modify the alloy while maintaining interphase-precipitation.
- Creep testing of vanadium steel should be carried out to provide concrete evidence that vanadium carbides limit the power-law creep mechanism of hydrogen attack.

Declaration of competing interest

The authors declare that they have no known competing financial interests or personal relationships that could have appeared to influence the work reported in this paper.

Acknowledgements

This work has been funded by the Oil & Gas Network Integrity division in the Research & Development Centre in Saudi Aramco. The authors would like to thank Diamond Light Source for beamtime (proposal MG28459), and the staff of beamlines I12 for assistance with testing and data collection.

REFERENCES

[1] Van Der Burg MWD, Van Der Giessen E, Brouwer RC. Investigation of hydrogen attack in 2.25Cr-1Mo steels with a high-triaxiality void growth model. Acta Metall 1996;44:505–18.
[2] Vagarali SS, Odette GR. A model for the growth of hydrogen attack cavities in carbon steels. Metall Trans A 1981;12(2071–2082).
[3] Parthasarathy TA. Mechanisms of hydrogen attack of carbon and 2.25Cr-1Mo steels. Acta Metall 1985;33:1673–81.
[4] Furtado HC, May IL. High temperature degradation in power plants and refineries. Mater Res 2004;7:103–10.
[5] Benac DJ, McAndrew P. Reducing the risk of high temperature hydrogen attack (HTHA) failures. J Fail Anal Prev 2012;12:624–7.
[6] Parthasarathy TA, Lopez HF, Shewmon PG. Hydrogen attack kinetics of 2.25Cr-1Mo steel weld metals. Metall Trans A 1985;16A:1143–9.
[7] Thygeson Jr JR, Molstad MC. High pressure hydrogen attack of steel. J Chem Eng Data 1964;9:309–15.
[8] Shewmon PG. Hydrogen attack of carbon steel. Metall Trans A 1976;7A:279–86.
[9] Eliezer D. High-temperature hydrogen attack of carbon steel. J Mater Sci 1981;16:2962–6.
[10] Kim TG. Failure of piping by hydrogen attack. Eng Fail Anal 2002;9:571–8.
[11] Martin ML, Dafarnia M, Orwig S, Moore D, Sofronis P. A microstructure- based mechanism of cracking in high temperature hydrogen attack. Acta Mater 2017;140:300–4.
[12] Chavoshi SZ, Hill LT, Bagnoli KE, Holloman RL, Nikbin KM. A combined fugacity and multi-axial ductility damage approach in predicting high temperature hydrogen attack in a reactor inlet nozzle. Eng Fail Anal 2020;117.
[13] Poorhaydari K. A comprehensive examination of high-temperature hydrogen attack – a review of over a century of investigations. J Mater Eng Perform 2021;30:7875–980.
[14] Anonymous. Catastrophic rupture of heat exchanger (seven fatalities). Techni- cal Report h9finery-fatal-explosion-and-fire/. Washington, D. C., USA: U. S. Chemical Safety and Hazard Investigation Board; 2014.
[15] Parthasarathy TA, Shewmon PG. Effects of tempering on the carbon activity and hydrogen attack kinetics of 2.25Cr-1Mo steel. Metall Trans A 1984;15:2021–7.
[16] Alshahrani MAM, Ooi SW, Hornqvist Colliander M, El Fallah GMAM, Bhadeshia HKDH. High-temperature hydrogen attack on 2.25cr-1mo steel: the roles of residual carbon, initial microstructure and carbide stability. Metall Mater Trans 2022;53:4221–32.
[17] Davenport AT, Berry FG, Honeycombe RWK. Interphase precipitation in iron alloys. Met Sci 1968;2:104–6.
[18] Bhadeshia HKDH, Honeycombe RWK. Steels: microstructure and properties. 4th ed. Elsevier; 2017.
[19] Dunlop GL, Honeycombe RWK. Ferrite morphologies and carbide precipitation in a Cr-Mo-V creep-resisting steel. Met Sci 1976;10:124–32.
[20] Miyamoto G, Hori R, Poorganji B, Furuhara T. Interphase precipitation of VC and resultant hardening in V-added medium carbon steels. ISIJ Int 2011;51:1733–9.
[21] Batte AD, Honeycombe RWK. Strengthening of ferrite by vanadium carbide precipitation. Met Sci 1973;7:160–8.
[22] Bhadeshia HKDH. Diffusional transformations: the nucleation of superledges. Phys Status Solidi 1982;69:745–50.
[23] Yen H-W, Chen P-Y, Huang C-Y, Yang J-R. Interphase precipitation of nanometer-sized carbides in a titanium–molybdenum-bearing low-carbon steel. Acta Mater 2011;59:6264–74.
[24] Lagneborg R, Siwecki T, Zajac S, Hutchinson B. The role of vanadium in microalloyed steels. Reprinted from The Scandanavian Journal of Metallurgy; 1999.
[25] Clark S, Janik V, Lan Y, Sridhar S. Interphase precipita- tion - an interfacial segregation model. ISIJ Int 2017. https://doi.org/10.2355/isijinternational.ISIJINT–2016–544.
[26] Tsai SP, Su TC, Yang JR, Chen CY, Wang YT, Huang CY. Effect of Cr and Al additions on the development of interphase-precipitated carbides strengthened dual-phase ti-bearing steels. Mater Des 2017;119:319–25.
[27] Lutterotti L. Materials analysis using diffraction. http://www.ing.unitn.it/maud/index.html. [Accessed 27 February 2013].
[28] Wang Z, Zhang Y, Miyamoto G, Furuhara T. Formation of abnormal nodular ferrite with interphase precipitation in a vanadium microalloyed low carbon steel. Scripta Mater 2021;198(113823).
[29] Bhadeshia HKDH. Bainite in steels: theory and practice. 3rd ed. Leeds, U.K.: Maney Publishing; 2015.
[30] Hucinska J. Advanced vanadium modified steels for high pressure hydrogen reactors. Adv Mater Sci 2003;4:21–7.
[31] Zhang S, Gross AF, van Atta SL, Lopez M, Liu P, Ahn CC, Vajo JJ, Jensen CM. The synthesis and hydrogen storage properties of a mgh_2 incorporated carbon aerogel scaffold. Nanotechnology April 2009;20.
[32] Ristic M, Ivanda M, Popovic S, Music S. Dependence of nanocrystalline sno_2 particle size on synthesis route. J Non-Cryst Solids 2002;303:270–80.